

TCAM: Temporal Class Activation Maps for Object Localization in Weakly-Labeled Unconstrained Videos

Soufiane Belharbi¹, Ismail Ben Ayed¹, Luke McCaffrey², and Eric Granger¹

¹ LIVIA, Dept. of Systems Engineering, ÉTS, Montreal, Canada

² Goodman Cancer Research Centre, Dept. of Oncology, McGill University, Montreal, Canada

soufiane.belharbi.1@ens.etsmtl.ca

ABSTRACT

Weakly supervised video object localization (WSVOL) allows locating object in videos using only global video tags such as object class. State-of-art methods rely on multiple independent stages, where initial spatio-temporal proposals are generated using visual and motion cues, then prominent objects are identified and refined. Localization is done by solving an optimization problem over one or more videos, and video tags are typically used for video clustering. This requires a model per-video or per-class making for costly inference. Moreover, localized regions are not necessary discriminant because of unsupervised motion methods like optical flow, or because video tags are discarded from optimization. In this paper, we leverage the successful class activation mapping (CAM) methods, designed for WSOL based on still images. A new Temporal CAM (TCAM) method is introduced to train a discriminant deep learning (DL) model to exploit spatio-temporal information in videos, using an aggregation mechanism, called CAM-Temporal Max Pooling (CAM-TMP), over consecutive CAMs. In particular, activations of regions of interest (ROIs) are collected from CAMs produced by a pre-trained CNN classifier to build pixel-wise pseudo-labels for training the DL model. In addition, a global unsupervised size constraint, and local constraint such as CRF are used to yield more accurate CAMs. Inference over single independent frames allows parallel processing of a clip of frames, and real-time localization. Extensive experiments¹ on two challenging YouTube-Objects datasets for unconstrained videos, indicate that CAM methods (trained on independent frames) can yield decent localization accuracy. Our proposed TCAM method achieves a new state-of-art in WSVOL accuracy, and visual results suggest that it can be adapted for subsequent tasks like visual object tracking and detection.

Keywords: Convolutional Neural Networks, Weakly Supervised Video Object Localization, Unconstrained Videos, Class Activation Maps (CAMs).

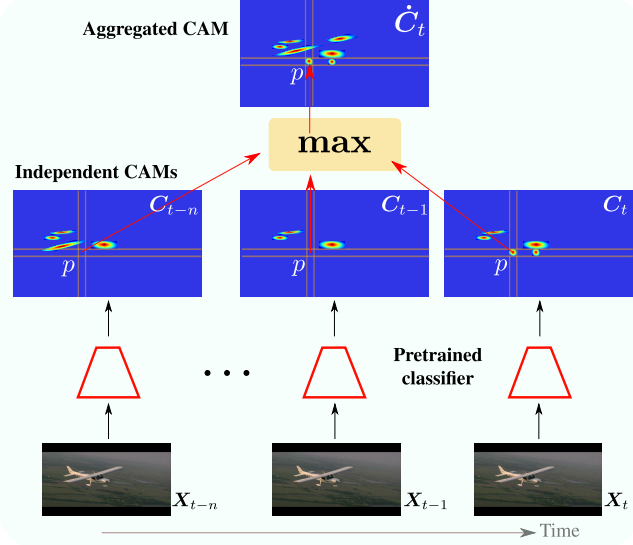


Figure 1: Example of CAM-Temporal Max Pooling (CAM-TMP) module for ROI aggregation of $n + 1$ consecutive CAMs generated by a pretrained CNN classifier. It takes maximum activation at location p across the independent CAMs to build the CAM, \dot{C}_t , that covers more discriminative parts. See notation in Sec.3.

1 Introduction

In recent years, a massive amount of videos can be easily accessed on the internet thanks to the rapid growth of video sharing platforms (Shao et al., 2022; Tang et al., 2013). Therefore, the need to develop automatic methods to process and analyze these videos is of a great interest. The object localization task in videos plays a critical role toward video content understanding. It can help improve the performance of subsequent tasks such as video summarization (Zhang et al., 2017), event detection (Chang et al., 2016), video object detection (Chen et al., 2020; Han et al., 2020; Shao et al., 2022), and visual object tracking (Bergmann et al., 2019; Luo et al., 2021).

Videos are often captured in the wild by non-professionals with varying quality, and mostly without constraints (moving objects and camera, viewpoint changes, decoding artifacts,

¹Code: <https://github.com/sbelharbi/tcam-wsol-video>.

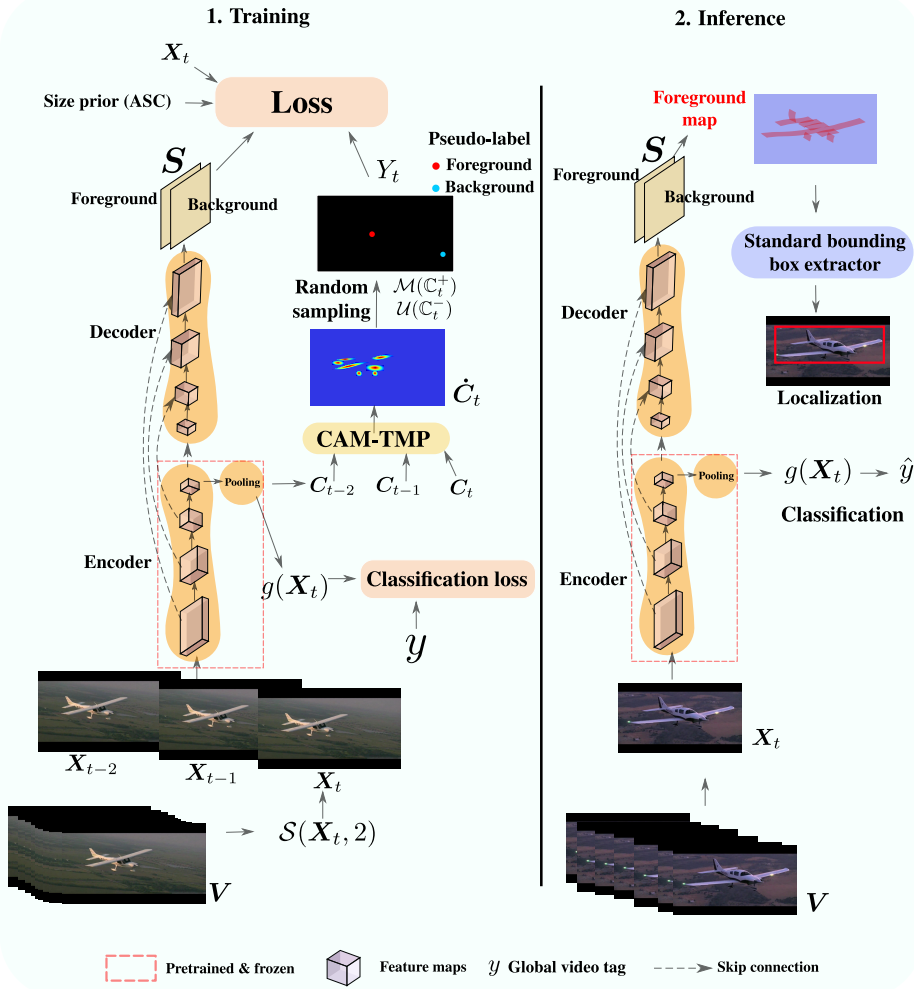


Figure 2: Our proposed TCAM. *Left*: training with temporal dependency $n = 2$. *Right*: inference (no temporal dependency). See notation in Sec.3.

and editing effects). However, while being abundant, exploiting these videos for down-stream tasks is still an ongoing challenge mainly due to the heavy annotation cost. Compared to still images, labeling videos represents a more difficult and expensive process, as videos often contain a large number of frames. For the object localization task, bounding boxes are required for each frame. Given this cost, videos are typically weakly-labeled (Jerripothula et al., 2016; Tsai et al., 2016) using tags (class). The weak label is defined for the entire video, and often describes the main object or concept occurring in the video without detailed spatio-temporal information. However, this yields noisy/corrupted labels since they are assigned to an entire video while only some of its frames may contain the object of interest. While such weak labels drastically reduce the annotation cost, it creates additional challenges for visual recognition tasks like object localization. Weakly-supervised learning has emerged as an important paradigm to leverage

coarse or global annotations like video-tags, mitigating the need for bounding boxes annotation. Despite the importance of WSVOL, it has seen limited research (Joulin et al., 2014; Koh et al., 2016; Kwak et al., 2015; Prest et al., 2012; Rochan et al., 2016; Zhang et al., 2020b). Instead, the literature on weakly supervised video object segmentation (WSVOS) has dominated (Croitoru et al., 2019; Fu et al., 2014; Haller and Leordeanu, 2017; Liu et al., 2014; Tsai et al., 2016; Tokmakov et al., 2016; Umer et al., 2021; Yan et al., 2017; Zhang et al., 2014), where bounding boxes are assumed to be produced via post-processing.

All the existing work are often conventional models, except (Croitoru et al., 2019; Tokmakov et al., 2016; Zhang et al., 2020b). They usually first generate spatio-temporal segments or proposals using visual and motion cues. Then, prominent objects are identified and refined using post-processing. While

these methods yield good performance, they present several limitations. All these methods require multiple sequential stages, and not trained in an end-to-end manner. Additionally, the solution often consists in optimizing over a single video or a cluster of videos of the same class. This is costly at inference time, and requires to build a model per-class or per-video which is cumbersome in practical applications, and scaled poorly to a large number of classes. Moreover, these methods are often non-discriminative. Video labels are not used *explicitly* in a differentiable way to extract objects; instead they are used only to cluster videos of same class. Consequentially, the localized object is not necessarily aligned *semantically* with the video tag. Similarly, since almost all methods use motion cues such as optical flow (Lee et al., 2011; Sundaram et al., 2010), they are prone to this alignment issue since such motion cues do not account for semantics. Lastly, motion information in unconstrained videos is very noisy due to movement of camera and objects.

To alleviate the aforementioned limitations, a new Temporal CAM (TCAM) method is proposed to train a single discriminative DL model through weakly-supervised learning. Our method requires only video tags without relying on additional assumptions. It is motivated by the success of weakly-supervised object localization (WSOL) methods for still images (Belharbi et al., 2022c; Choe and Shim, 2019; Durand et al., 2017; Gao et al., 2021; Jiang et al., 2021; Singh and Lee, 2017; Wei et al., 2021; Zhou et al., 2016). Currently, many WSOL tasks are addressed using Class Activation Mappings (CAM) methods (Zhou et al., 2016). Using only global class labels, CAM methods allow training a CNN classifier end-to-end, in a differentiable way, to spatially localize the discriminative ROI in an image. Consequentially, localized ROI are aligned with the semantic label of the image. At inference time, a trained model can rapidly classify an image and localized the corresponding ROI, and scale well to a large number of classes, making it practical for real-world applications. However, these methods are limited to single images, and cannot exploit the temporal dependency between images in videos. To leverage spatio-temporal information, we propose a new CAM Temporal Max-Pooling (CAM-TMP) mechanism allowing aggregation the ROIs from a sequence of CAMs (Fig.1). Our CAM-TMP simulates *union* operation over ROIs in each frame by gathering ROIs from each CAM, providing a better coverage of an object.

Our TCAM method relies on a U-Net style architecture (Ronneberger et al., 2015) to classify an image and localize the corresponding ROI through full-resolution CAMs for better accuracy (Fig.2). Using a pre-trained CNN to classify successive frames, we train our DL model over a *sequence* of frames, where CAM-TMP is used to accumulate ROIs that are employed to generate better pseudo-labels for training at pixel-level. Following common practice (Durand et al., 2017;

Zhou et al., 2016), strong activations in a CAM are considered foreground, while low activations are background. At each Stochastic Gradient Descent (SGD) step, we randomly sample a foreground (FG) and background (BG) pixel pseudo-label in each input image (Belharbi et al., 2022c;a). Such random sampling allows exploring FG/BG regions, and promotes the emergence of consistent CAMs. In contrast to independent CAMs, our CAM-TMP builds CAMs that covers better objects which leads to better sampling. To mitigate common issues of CAMs such as small ROI, we use unsupervised size prior (Belharbi et al., 2022c;a;b; Pathak et al., 2015) as a global constraints to encourage growth of both FG and BG regions, and avoid learning unbalanced CAMs. CRF loss (Tang et al., 2018) is also used to align CAMs with object boundaries by leveraging statistical properties of the image such as pixel color and proximity between pixels. Inference in our method is performed over independent frames without considering temporal dependencies, allowing real-time inference.

To the best of our knowledge, this is the first CAM-method in WSVOL task. Our work aims to push ahead state-of-the-art performance in this task, while re-animating the recent stalling research in this field.

Our main contributions are summarized as follows.

(1) A TCAM method is proposed for WSVOL task. Different from existing method, our TCAM method builds single discriminative DL model able to process all classes at once. In addition, inference is done over independent frames allowing for real-time inference. TCAM is able to produce the bounding box location of an object estimated from CAMs, along with corresponding class prediction. Training with our method is achieved over unconstrained videos using only their global class-tag, and without any additional assumptions.

(2) Unlike standard CAMs which are limited to still images, TCAM leverages spatio-temporal information in a sequence of CAMs. Using temporal max-pooling (CAM-TMP) module, we are able to extract relevant ROIs from a sequence of generic CAMs provided by a pretrained CNN classifier. CAM-TMP then yields a single accurate CAM with better coverage of an object. Our loss exploit this CAM for training our deep model by sampling random foreground/background regions. Additional constraint losses, including size prior and CRF, are used to obtained balanced and accurate CAMs. Note that our TCAM is generic, and can be integrated on top of any CAM method.

(3) Extensive experiments conducted on two public benchmarks of unconstrained videos, YouTube-Objects v1.0 and v2.2 datasets showed that: (a) simple CAM methods designed for still images for WSOL task can achieve a high level of localization accuracy on test set videos; (b) our TCAM method achieve state-of-art in WSVOL accuracy. We note that TCAM

can be adapted for subsequent challenging tasks such as visual object tracking and detection.

2 Related Work

Weakly Supervised Video Object Localization. The limited amount of research in this category are often based on non-discriminative and non-deep models. These methods (Koh et al., 2016; Kwak et al., 2015; Prest et al., 2012; Rochan et al., 2016; Zhang et al., 2020b) initialize and select prominent proposals to be refined while considering spatio-temporal consistency constraints using mainly visual appearance and motion features. Different methods use prominent proposals as supervision to train a localizer (Prest et al., 2012; Zhang et al., 2020b). Others rely on segmentation (Rochan et al., 2016) followed by additional refinement using GrabCut (Rother et al., 2004). Single or cluster of videos are considered at once for optimization. For instance, POD method (Koh et al., 2016) considers an iterative approach to localize a primary object in a video assumed to appear in most frames but not in all frames. It is achieved while empty frames are identified. Region proposals are initially generated via (Alexe et al., 2012). Each proposal is bisected into foreground and background. Models for foreground, background, and primary object are built. An iterative scheme is setup to refine each model in an evolutionary manner. The final primary model is used to select candidate proposals and locate the bounding box. Recently, SPFTN (Zhang et al., 2020b) considers a deep learning framework that jointly learns to segment and localize objects with noisy supervision estimation using advanced optical flow (Lee et al., 2011). Self-paced learning is considered to alleviate the ambiguity/noisy supervision. Other methods (Joulin et al., 2014) rely on co-localization of common object over a set of videos or images.

Weakly Supervised Video Object Segmentation. Most methods are non-deep and non-discriminative based models. They undergo multiple steps to perform segmentation. They often operate on a single video or a cluster of videos, and bounding boxes are obtained via post-processing.

A set of methods initiate the learning by extracting independent spatio-temporal segments (Hartmann et al., 2012; Tang et al., 2013; Xu et al., 2012; Yan et al., 2017) using for instance unsupervised methods (Banica et al., 2013; Xu et al., 2012) or generate proposals (Zhang et al., 2015) using pre-trained detectors (Zhang et al., 2015). These object-parts are then gathered using different features which mainly include visual appearance and motion cues while preserving temporal consistency. This is often done using graph-based models such as Conditional random field (CRF) or GrabCut-like approach (Rother et al., 2004). Deep models are rarely used. For instance, Authors in (Liu et al., 2014) propose a nearest neighbor-based label transfer between videos to deal with

multi-class video segmentation. Videos are first segmented into spatio-temporal supervoxels (Xu et al., 2012) which then represented in high dimensional feature space using color, texture, and motion. A multi-video graph is built, and using appearance, this graph model encourages label smoothness between spatio-temporal adjacent supervoxels in the same video and supervoxels with similar appearance across other videos. This yields a final pixel segmentation. M-CNN (Tokmakov et al., 2016) combines motion cues with a fully convolutional network (FCN). A Gaussian mixture model is used to estimate foreground appearance potentials via motion (Papazoglou and Ferrari, 2013). These potentials are combined with the FCN prediction to estimate label predictions of foreground using GrabCut-like approach (Rother et al., 2004). These labels are used to fit the FCN. Authors use a fine-tuning stage over only few videos.

Other methods leverage co-segmentation to segment an object based on its occurrence on multiple images. A dominant approach is to use inter- and intra videos visual and motions cues to find common segments. Graphs, such as CRF and graph cuts, are used to model relations between variant segments (Chen et al., 2012; Fu et al., 2014; Tsai et al., 2016; Zhang et al., 2014). For example, authors in (Tsai et al., 2016) generate object-like tracklets using a pretrained FCN. After collecting tracklets from all videos, they are linked for each object category via a graph. A sub-modular optimization is formulated to define the corresponding relation between tracklets based on their similarities while accounting for object properties such as appearance, shape, and motion. After maximizing this sub-modular function, tracklets are ranked using their mutual similarities allowing discovery of prominent objects in each video.

While all previous methods use labels to cluster videos of the same class, other methods do not use labels. However, the general process is roughly the same since previous methods do not exploit labels explicitly in their optimization. An initial guess of foreground regions is estimated (Croitoru et al., 2019; Haller and Leordeanu, 2017; Papazoglou and Ferrari, 2013; Umer et al., 2021). This is achieved either using motion cues via (Sundaram et al., 2010) such as in (Papazoglou and Ferrari, 2013), Principal Component Analysis (PCA) such in (Haller and Leordeanu, 2017; Umer et al., 2021), or using VideoPCA algorithm (Stretcu and Leordeanu, 2015) as in (Croitoru et al., 2019). This initial guess is not necessarily discriminative. A final segmentation is then obtained by refinement using graphs (Rother et al., 2004). For instance, authors in (Croitoru et al., 2019) propose a deep-based model. It is based on an iterative learning process where at each iteration, a CNN teacher is trained to discover object in videos. Object discovery is achieved using VideoPCA algorithm (Stretcu and Leordeanu, 2015) which leverages spatio-temporal consistency in videos using appearance, shape, movement, and location of objects.

Estimated foreground by the the teacher are fed to a CNN student for supervised training. Through iteration, several students are built and replace object discovery providing more reliable object segmentation.

Weakly Supervised Object Localization in Still Images. Early work in WSOL (Rony et al., 2022) focused on designing different spatial pooling layers. This includes Global Average Pooling (GAP) (Lin et al., 2013), weighed GAP (Zhou et al., 2016), max-pooling (Oquab et al., 2015), LSE (Pinheiro and Collobert, 2015; Sun et al., 2016), PRM (Zhou et al., 2018), WILDCAT (Durand et al., 2017; 2016), and multi-instance learning pooling (MIL) (Ilse et al., 2018). However, very quickly, these methods hit their limitation where the produced CAMs can cover only small discriminative parts of the object. Subsequent work aimed to improve this aspect by refining the CAMs. This achieved through three different ways: (1) *via data augmentation* by perturbing input image such as in HaS (Singh and Lee, 2017), CutMix (Yun et al., 2019), AE (Wei et al., 2017), ACoL (Zhang et al., 2018b), MEIL (Mai et al., 2020), and MaxMin (Belharbi et al., 2022b); or by perturbing features as in SPN (Zhu et al., 2017), GAIN (Li et al., 2018), and ADL (Choe and Shim, 2019), or (2) *via architectural changes* such as in NL-CCAM (Yang et al., 2020), FickleNet (Lee et al., 2019), DANet (Xue et al., 2019), I²C (Zhang et al., 2020c), ICL (Ki et al., 2020), and TS-CAM (Gao et al., 2021), or (3) *by using pseudo-labels for fine-tuning* such as in SPG (Zhang et al., 2018c), PSOL (Zhang et al., 2020a), SPOL (Wei et al., 2021), FCAM (Belharbi et al., 2022c), and NEGEV (Belharbi et al., 2022a). Other methods aim to produce the bounding box directly without CAMs (Meethal et al., 2020). All the aforementioned methods extract localization from forward pass in the model. Other methods rely on forward and backward pass to estimate CAMs. This includes methods that (1) *are biologically inspired* such as feedback layer (Cao et al., 2015), and Excitation-backprop (Zhang et al., 2018a), or (2) *rely on gradient-aggregation* such as GradCAM (Selvaraju et al., 2017), GradCam++ (Chattopadhyay et al., 2018), XGradCAM (Fu et al., 2020), and Layer-CAM (Jiang et al., 2021), or (3) *use confident-aggregation* to avoid gradient saturation (Adebayo et al., 2018; Kindermans et al., 2019) such as Ablation-CAM (Desai and Ramaswamy, 2020), Score-CAM (Wang et al., 2020), SS-CAM (Naidu and Michael, 2020), and IS-CAM (Naidu et al., 2020). Despite the success of these methods, they are limited to still images and they are not equipped to leverage temporal information in videos.

Our proposal benefits from the simplicity of CAM methods, which provide single discriminative DL model for the WSOL task, to mitigate several issues in WSVOL. In addition, our TCAM method leverages the spatio-temporal information in videos.

3 Proposed Approach

Notation. Let $\mathbb{D} = \{(\mathbf{V}, y)_i\}_{i=1}^N$ denotes a training set of videos, where $\mathbf{V} = \{\mathbf{X}_t\}_{t=1}^z$ is an input video with z frames, and $\mathbf{X}_t : \Omega \subset \mathbb{R}^2$ is the t th frame in the video; $y \in \{1, \dots, K\}$ is the video global class label, with K the number of classes. Assume that all frames inherit the same class label as the video global class tag. Our model is a U-Net style architecture (Ronneberger et al., 2015) (Fig.2). It is composed of two parts: (a) classification module g with parameters \mathbf{W} . It performs image classification. (b) segmentation module (decoder) f with parameters θ . It outputs two CAMs, one for the foreground and the other for background. The classifier g is composed of an encoder backbone for building features, and a pooling head to yield classification scores. We denote by $g(\mathbf{X}) \in [0, 1]^K$ the per-class classification probabilities where $g(\mathbf{X})_k = \Pr(k|\mathbf{X})$. The classifier g is trained using standard cross-entropy to correctly classify independent frames, $\min_{\mathbf{W}} -\log(g(\mathbf{X})[y])$.

Once trained, its weights \mathbf{W} are frozen, and not considered for future training. Classifier g can yield a CAM of the target y , referred to as \mathbf{C} . We note \mathbf{C}_t as the corresponding CAM of the the frame \mathbf{X}_t at time t . The decoder generates softmax activation maps denoted as $\mathbf{S}_t = f(\mathbf{X}_t) \in [0, 1]^{|\Omega| \times 2}$. Note that $\mathbf{S}_t^0, \mathbf{S}_t^1$ refer to the background and foreground maps, respectively. Let $\mathbf{S}_t(p) \in [0, 1]^2$ denotes a row of matrix \mathbf{S}_t , with index $p \in \Omega$ indicating a point within Ω . The operation $\mathcal{S}(\cdot, n)$ provides the set of n previous neighbors of an element in the same video, plus the element itself. For instance, $\mathcal{S}(\mathbf{X}_t, n) = \{\mathbf{X}_t, \mathbf{X}_{t-1}, \dots, \mathbf{X}_{t-n}\}$ is the set of n previous frames of the frame \mathbf{X}_t , and $\mathcal{S}(\mathbf{C}_t, n) = \{\mathbf{C}_t, \mathbf{C}_{t-1}, \dots, \mathbf{C}_{t-n}\}$ is the set of n previous CAMs of the CAM \mathbf{C}_t .

CAM Temporal Max-Pooling (CAM-TMP). A sequence of frames in a video often captures the same scene with minimal variations. Therefore, objects within the scene have small displacement. However, this small change can cause CAMs to vary slightly, and highlight different minimal parts of the object as ROI. We leverage this behavior to build a single CAM, $\dot{\mathbf{C}}_t$, that covers more parts at once. This CAM will be used later for sampling foreground/background regions. To this end, we propose an aggregation method between consecutive CAMs where we perform a *union* operation between all spotted ROI in each CAM. This is achieved by taking the *maximum* CAM activation through time over activation in the same position of a sequence of CAMs (Fig.1). This is similar to spatial max-pooling operation, commonly used in CNNs, that seeks the presence of the object in small spatial neighborhood. Our temporal max-pooling seeks to determine whether one of the CAMs has activated over the object in a sequence of CAMs. At spatial position p , we formulate our CAM-TMP by taking the maximum across all CAMs at the

same position,

$$\dot{\mathbf{C}}_t(p) = \max\{\mathbf{C}^1(p), \dots, \mathbf{C}^{n+1}(p)\}, \mathbf{C}^i \in \mathcal{S}(\mathbf{C}_t, n), \quad (1)$$

where \mathbf{C}^i is the i th element of the set $\mathcal{S}(\mathbf{C}_t, n)$, and $p \in \Omega$.

Sampling Pseudo-Labels. To guide the training of the decoder f , we exploit pixel-wise pseudo-supervision collected from the previously built CAM $\dot{\mathbf{C}}_t$ for the corresponding frame \mathbf{X}_t . We rely on the common assumption that strong activations in a CAM are more likely to be foreground, and low activations are considered background (Belharbi et al., 2022c;a; Durand et al., 2017; Zhou et al., 2016). We denote \mathbb{C}_t^+ as foreground region, estimated via the operation \mathcal{O}^+ . It is determined as pixels with activations greater than Otsu threshold (Otsu, 1979) estimated over $\dot{\mathbf{C}}_t$. The leftover region, estimated via the operation \mathcal{O}^- , is considered more likely background \mathbb{C}_t^- .

$$\mathbb{C}_t^+ = \mathcal{O}^+(\dot{\mathbf{C}}_t), \quad \mathbb{C}_t^- = \mathcal{O}^-(\dot{\mathbf{C}}_t). \quad (2)$$

Both foreground and background regions are noisy and uncertain. The region \mathbb{C}_t^- is still likely to contain part of the object. Similarly, \mathbb{C}_t^+ may still contain background. Due to this uncertainty, we avoid to directly fit these regions to the model. Instead, we consider a stochastic sampling over each region to avoid overfitting and allow the emergence of consistent regions (Belharbi et al., 2022c;a). For each frame, and at each SGD step, we randomly select one pixel as foreground pseudo-label, and another single pixel as background pseudo-label. Their location is represented in,

$$\Omega'_t = \mathcal{M}(\mathbb{C}_t^+) \cup \mathcal{U}(\mathbb{C}_t^-), \quad (3)$$

where $\mathcal{M}(\mathbb{C}_t^+)$ is a multinomial sampling distribution function over foreground region that samples a single location using the magnitude of pixels activations located exclusively in \mathbb{C}_t^+ . Therefore, strong activation are more likely to be sampled as foreground.

Uniform sampling distribution $\mathcal{U}(\mathbb{C}_t^-)$ is used to sample a single background pixel from \mathbb{C}_t^- . We favor uniform random exploration of background region since the background is evenly distributed over the image. However, foreground region is only distributed over one place where the object is located. We denote by Y_t the *partially* pseudo-labeled mask for the sample \mathbf{X}_t , where $Y_t(p) \in \{0, 1\}^2$ with labels 0 for background, and 1 for foreground. This mask holds the sampled locations in Eq. 3 and their pseudo-labels. Locations with unknown pseudo-labels are encoded as unknown.

Overall Training Loss. Our training loss considers a frame \mathbf{X}_t and its n previous frames, *i.e.* $\mathcal{S}(\mathbf{X}_t, n)$, to leverage spatio-temporal information in a video. The time position t is uniformly and randomly sampled in the video. The loss is composed of three parts. **a)** pixel-wise alignment using

pseudo-label Y_t . This is achieved using partial cross-entropy,

$$\begin{aligned} \mathbf{H}_p(Y_t, \mathbf{S}_t) = & \\ & - (1 - Y_t(p)) \log(1 - \mathbf{S}_t^0(p)) - Y_t(p) \log(\mathbf{S}_t^1(p)). \end{aligned} \quad (4)$$

b) To avoid the common unbalanced problem CAMs \mathbf{S}_t , where the background dominates the foreground (or the opposite), a global constraint is considered – the absolute size constraint (ASC) (Belharbi et al., 2022b) over both regions. We do not assume whether the background is larger than the foreground (Pathak et al., 2015) nor the opposite. This constraint pushes both regions to be large, and it is formulated as inequality constraints which are then solved via a standard log-barrier method (Boyd and Vandenberghe, 2004). **c)** To avoid trivial solution of ASC, where half the image is foreground and the other half is background, we use an additional local term that leverage pixels statistics including color and proximity. In particular, the CRF loss (Tang et al., 2018), denoted by \mathcal{R} is included to ensure that CAM activations are consistent with the object boundaries and sampling regions.

Our overall total loss is formulated as,

$$\begin{aligned} \min_{\theta} \quad & \sum_{p \in \Omega'_t} \mathbf{H}_p(Y_t, \mathbf{S}_t) + \lambda \mathcal{R}(\mathbf{S}_t, \mathbf{X}_t), \\ \text{s.t.} \quad & \sum \mathbf{S}_t^r \geq 0, \quad r \in \{0, 1\}, \end{aligned} \quad (5)$$

where $\sum \mathbf{S}_t^0, \sum \mathbf{S}_t^1$ are the area size of the background and foreground regions, respectively.

The training of our method (Eq. 5) only requires the video global tag y to train the classifier g , and properly estimate the pseudo-label mask Y_t corresponding to the correct object class labeled in the video. This ensures that the semantic meaning of the foreground in \mathbf{S}_t^1 is aligned with the true label y . The spatio-temporal dependency between CAMs is leveraged in Eq. 1 to compute $\dot{\mathbf{C}}_t$ which is then used to sample Y_t . Our final trained model is evaluated on single independent frames, thereby producing a class prediction for the object in the frame, along with its spatial localization \mathbf{S}_t^1 . Therefore, frames can be processed in parallel saving more inference time. Standard methods may be used for bounding box estimation in CAMs (Fig. 2, right) (Choe et al., 2020).

4 Results and Discussion

4.1 Experimental Methodology

Datasets. For evaluation, we perform experiments on unconstrained video datasets for WSVOL task where videos are labeled globally using class label for training, and frame bounding boxes are provided for evaluation. In particular, we consider two public challenging datasets: YouTube-Object v1.0 (YTOv1 (Prest et al., 2012)) and v2.2 (YTOv2.2 (Kalogeiton et al., 2016)) datasets. We follow common protocol for WSVOL task (Kalogeiton et al., 2016; Prest et al., 2012).

| Datasets | Methods | Aero | Bird | Boat | Car | Cat | Cow | Dog | Horse | Mbikes | Train | Avg | Time/Frame |
|----------|---|-------------|-------------|-------------|-------------|-------------|-------------|-------------|-------------|-------------|-------------|-------------|------------|
| YTOv1 | (Prest et al., 2012) (cvpr,2012) | 51.7 | 17.5 | 34.4 | 34.7 | 22.3 | 17.9 | 13.5 | 26.7 | 41.2 | 25.0 | 28.5 | N/A |
| | (Papazoglou and Ferrari, 2013) (iccv,2013) | 65.4 | 67.3 | 38.9 | 65.2 | 46.3 | 40.2 | 65.3 | 48.4 | 39.0 | 25.0 | 50.1 | 4s |
| | (Joulin et al., 2014) (eccv,2014) | 25.1 | 31.2 | 27.8 | 38.5 | 41.2 | 28.4 | 33.9 | 35.6 | 23.1 | 25.0 | 31.0 | N/A |
| | (Kwak et al., 2015) (iccv,2015) | 56.5 | 66.4 | 58.0 | 76.8 | 39.9 | 69.3 | 50.4 | 56.3 | 53.0 | 31.0 | 55.7 | N/A |
| | (Rochan et al., 2016) (ivc,2016) | 60.8 | 54.6 | 34.7 | 57.4 | 19.2 | 42.1 | 35.8 | 30.4 | 11.7 | 11.4 | 35.8 | N/A |
| | (Tokmakov et al., 2016) (eccv,2016) | 71.5 | 74.0 | 44.8 | 72.3 | 52.0 | 46.4 | 71.9 | 54.6 | 45.9 | 32.1 | 56.6 | N/A |
| | POD (Koh et al., 2016) (cvpr,2016) | 64.3 | 63.2 | 73.3 | 68.9 | 44.4 | 62.5 | 71.4 | 52.3 | 78.6 | 23.1 | 60.2 | N/A |
| | (Tsai et al., 2016) (eccv,2016) | 66.1 | 59.8 | 63.1 | 72.5 | 54.0 | 64.9 | 66.2 | 50.6 | 39.3 | 42.5 | 57.9 | N/A |
| | (Haller and Leordeanu, 2017) (iccv,2017) | 76.3 | 71.4 | 65.0 | 58.9 | 68.0 | 55.9 | 70.6 | 33.3 | 69.7 | 42.4 | 61.1 | 0.35s |
| | (Croitoru et al., 2019) (LowRes-Net _{iter1}) (ijcv,2019) | 77.0 | 67.5 | 77.2 | 68.4 | 54.5 | 68.3 | 72.0 | 56.7 | 44.1 | 34.9 | 62.1 | 0.02s |
| | (Croitoru et al., 2019) (LowRes-Net _{iter2}) (ijcv,2019) | 79.7 | 67.5 | 68.3 | 69.6 | 59.4 | 75.0 | 78.7 | 48.3 | 48.5 | 39.5 | 63.5 | 0.02s |
| | (Croitoru et al., 2019) (DilateU-Net _{iter2}) (ijcv,2019) | 85.1 | 72.7 | 76.2 | 68.4 | 59.4 | 76.7 | 77.3 | 46.7 | 48.5 | 46.5 | 65.8 | 0.02s |
| | (Croitoru et al., 2019) (MultiSelect-Net _{iter2}) (ijcv,2019) | 84.7 | 72.7 | 78.2 | 69.6 | 60.4 | 80.0 | 78.7 | 51.7 | 50.0 | 46.5 | 67.3 | 0.15s |
| | SPFTN (M) (Zhang et al., 2020b) (tpami,2020) | 66.4 | 73.8 | 63.3 | 83.4 | 54.5 | 58.9 | 61.3 | 45.4 | 55.5 | 30.1 | 59.3 | N/A |
| | SPFTN (P) (Zhang et al., 2020b) (tpami,2020) | 97.3 | 27.8 | 81.1 | 65.1 | 56.6 | 72.5 | 59.5 | 81.8 | 79.4 | 22.1 | 64.3 | N/A |
| | FPPVOS (Umer et al., 2021) (optik,2021) | 77.0 | 72.3 | 64.7 | 67.4 | 79.2 | 58.3 | 74.7 | 45.2 | 80.4 | 42.6 | 65.8 | 0.29s |
| | CAM (Zhou et al., 2016) (cvpr,2016) | 75.0 | 55.5 | 43.2 | 69.7 | 33.3 | 52.4 | 32.4 | 74.2 | 14.8 | 50.0 | 50.1 | 0.2ms |
| | GradCAM (Selvaraju et al., 2017) (iccv,2017) | 86.9 | 63.0 | 51.3 | 81.8 | 45.4 | 62.0 | 37.8 | 67.7 | 18.5 | 50.0 | 56.4 | 27.8ms |
| | GradCAM++ (Chattopadhyay et al., 2018) (wacv,2018) | 79.8 | 85.1 | 37.8 | 81.8 | 75.7 | 52.4 | 64.9 | 64.5 | 33.3 | 56.2 | 63.2 | 28.0ms |
| | Smooth-GradCAM++ (Omeiza et al., 2019) (corr,2019) | 78.6 | 59.2 | 56.7 | 60.6 | 42.4 | 61.9 | 56.7 | 64.5 | 40.7 | 50.0 | 57.1 | 136.2ms |
| | XGradCAM (Fu et al., 2020) (bmvc,2020) | 79.8 | 70.4 | 54.0 | 87.8 | 33.3 | 52.4 | 37.8 | 64.5 | 37.0 | 50.0 | 56.7 | 14.2ms |
| | LayerCAM (Jiang et al., 2021) (ieee,2021) | 85.7 | 88.9 | 45.9 | 78.8 | 75.5 | 61.9 | 64.9 | 64.5 | 33.3 | 56.2 | 65.6 | 17.9ms |
| | TCAM (ours) | 90.5 | 70.4 | 62.2 | 75.7 | 84.8 | 81.0 | 81.0 | 64.5 | 70.4 | 50.0 | 73.0 | 18.5ms |
| YTOv2.2 | (Haller and Leordeanu, 2017) (iccv,2017) | 76.3 | 68.5 | 54.5 | 50.4 | 59.8 | 42.4 | 53.5 | 30.0 | 53.5 | 60.7 | 54.9 | 0.35s |
| | (Croitoru et al., 2019) (LowRes-Net _{iter1}) (ijcv,2019) | 75.7 | 56.0 | 52.7 | 57.3 | 46.9 | 57.0 | 48.9 | 44.0 | 27.2 | 56.2 | 52.2 | 0.02s |
| | (Croitoru et al., 2019) (LowRes-Net _{iter2}) (ijcv,2019) | 78.1 | 51.8 | 49.0 | 60.5 | 44.8 | 62.3 | 52.9 | 48.9 | 30.6 | 54.6 | 53.4 | 0.02s |
| | (Croitoru et al., 2019) (DilateU-Net _{iter2}) (ijcv,2019) | 74.9 | 50.7 | 50.7 | 60.9 | 45.7 | 60.1 | 54.4 | 42.9 | 30.6 | 57.8 | 52.9 | 0.02s |
| | (Croitoru et al., 2019) (BasicU-Net _{iter2}) (ijcv,2019) | 82.2 | 51.8 | 51.5 | 62.0 | 50.9 | 64.8 | 55.5 | 45.7 | 35.3 | 55.9 | 55.6 | 0.02s |
| | (Croitoru et al., 2019) (MultiSelect-Net _{iter2}) (ijcv,2019) | 81.7 | 51.5 | 54.1 | 62.5 | 49.7 | 68.8 | 55.9 | 50.4 | 33.3 | 57.0 | 56.5 | 0.15s |
| | CAM (Zhou et al., 2016) (cvpr,2016) | 52.3 | 66.4 | 25.0 | 66.4 | 39.7 | 87.8 | 34.7 | 53.6 | 45.4 | 43.7 | 51.5 | 0.2ms |
| | GradCAM (Selvaraju et al., 2017) (iccv,2017) | 44.1 | 68.4 | 50.0 | 61.1 | 51.8 | 79.3 | 56.0 | 47.0 | 44.8 | 42.4 | 54.5 | 27.8ms |
| | GradCAM++ (Chattopadhyay et al., 2018) (wacv,2018) | 74.7 | 78.1 | 38.2 | 69.7 | 56.7 | 84.3 | 61.6 | 61.9 | 43.0 | 44.3 | 61.2 | 28.0ms |
| | Smooth-GradCAM++ (Omeiza et al., 2019) (corr,2019) | 74.1 | 83.2 | 38.2 | 64.2 | 49.6 | 82.1 | 57.3 | 52.0 | 51.1 | 42.4 | 59.5 | 136.2ms |
| | XGradCAM (Fu et al., 2020) (bmvc,2020) | 68.2 | 44.5 | 45.8 | 64.0 | 46.8 | 86.4 | 44.0 | 57.0 | 44.9 | 45.0 | 54.6 | 14.2ms |
| | LayerCAM (Jiang et al., 2021) (ieee,2021) | 80.0 | 84.5 | 47.2 | 73.5 | 55.3 | 83.6 | 71.3 | 60.8 | 55.7 | 48.1 | 66.0 | 17.9ms |
| | TCAM (ours) | 79.4 | 94.9 | 75.7 | 61.7 | 68.8 | 87.1 | 75.0 | 62.4 | 72.1 | 45.0 | 72.2 | 18.5ms |

Table 1: Localization performance (CorLoc) on the YTOv1 (Prest et al., 2012) and YTOv2.2 (Kalogeiton et al., 2016) test sets.

YouTube-Object v1.0 (YTOv1) (Prest et al., 2012): This dataset is composed of videos collected from YouTube² by querying for the names of 10 object classes. Each class has between 9 and 24 videos with a duration that varies from 30 seconds to 3 minutes. It contains 155 videos where each video is split into short duration clips named shots. There are 5507 shots, with each gathering multiple frames, reaching in total 571 089 frames. In each shot, only few frames are annotated with a bounding box to localized object of interest. The authors divided the dataset into 27 testing videos with a total of 396 labeled bounding boxes, and 128 video for training. It is common to use part of the training videos as validation set. In our experiments, we consider 5 random videos per class which amounts to a total of 50 videos for validation.

YouTube-Object v2.2 (YTOv2.2) (Kalogeiton et al., 2016): This is an extension and improvement of YTOv1. It contains more frames, 722 040 frames in total. More importantly, authors provided more bounding boxes annotations. They divided the dataset into 106 videos for training, and 49 videos for test. For validation set, we consider, in our case, 3 random videos per class from the trainset. Compared to YTOv1, the test set contains much more annotation. It holds 1 781 frames with bounding boxes annotation, and a total of 2 667 bounding boxes. This makes this release much more challenging.

Evaluation Measure. For localization performance, CorLoc metric (Deselaers et al., 2012) is used. It represents the percentage of predicted bounding boxes that have an Intersection Over Union (IoU) between prediction and ground truth greater than half ($\text{IoU} > 50\%$). In addition, standard classification accuracy, CL, is used to measure classification performance. It is measured over frames with bounding boxes.

Implementations Details. In all our experiments, we train for 100 epochs with 32 mini-batch size. Following WSOL task (Choe et al., 2020), we used ResNet50 (He et al., 2016) as a backbone. Images are resized to 256×256 , then randomly cropped to 224×224 for training. The temporal dependency n in Eq.1 is set via the validation set from the set $n \in \{1, \dots, 10\}$. In Eq.5, the hyper-parameter λ for the CRF is set to the same value as in (Tang et al., 2018) that is $2e^{-9}$. For log-barrier optimization, hyper-parameter t is set to the same value as in (Belharbi et al., 2019; Kervadec et al., 2019). It is initialized to 1, and increased by a factor of 1.01 in each epoch with a maximum value of 10. In all experiments, we used a learning rate in $\{0.1, 0.01, 0.001\}$ using SGD for optimization. Our classifier is pretrained on independent frames. In all our experiments, and due to the large number of redundant frames per video, we randomly select a different frame in each shot at each epoch. This allows training deep models over videos in a reasonable time.

Baseline Methods. For validation, we compare our method to available results. In particular, we compare to (Croitoru et al., 2019; Haller and Leordeanu, 2017; Joulin et al., 2014; Kwak et al., 2015; Papazoglou and Ferrari, 2013; Prest et al., 2012; Rochan et al., 2016; Tokmakov et al., 2016; Tsai et al., 2016), POD (Koh et al., 2016), SPFTN (Zhang et al., 2020b), and FPPVOS (Umer et al., 2021). Additionally, we implemented several CAM-based methods for further comparison. This includes CAM (Zhou et al., 2016), GradCAM (Selvaraju et al., 2017), GradCam++ (Chattopadhyay et al., 2018), Smooth-GradCAM++ (Omeiza et al., 2019), XGradCAM (Fu et al., 2020), and LayerCAM (Jiang et al., 2021). CAM-based methods are trained on independent frames. In all our experiments, we use LayerCAM (Jiang et al., 2021) to generate CAMs used to build a complete CAM $\hat{C}_t(p)$ (Eq.1), which is then used to build pseudo-labels Y_t (Eq.5). Note that our method is generic. It can be used with any CAM method.

4.2 Results

Comparison with State-of-Art. Tab. 1 presents the results obtained on both datasets YTOv1, and YTOv2.2. We first note that CAM-based methods are very competitive compare to previous state-of-the-art methods. In particular, GradCAM++ (Chattopadhyay et al., 2018) and LayerCAM (Jiang et al., 2021) achieved an average localization performance of CorLoc of 63.1%, 65.6% over YTOv1, and 61.2%, 66.0% over YTOv2.2, respectively. Previous state-of-the-art methods yielded 67.3%, and 56.5%, respectively. This demonstrates the benefit of discriminative training of CAMs even though they are not aware of temporal dependency. Training our CAM-based method with temporal awareness between frames has boosted the localization performance furthermore reaching new state-of-the-art results. The same table shows as well that all methods suffer a discrepancy in performance between different objects where some classes are easier than others. For instance, the class 'train' seems very difficult. In CAM-based methods, we noticed that 'train' localization is often mistaken with railway track since they often co-occur together. In addition, this object is often filmed from close range, at stations, leading to a large object, that often covers the entire frame making its localization difficult.

Although it is not commonly provided, we present classification performance in Tab.2 for our trained CAM-methods since they are able to do both tasks: classification, and localization. These methods yielded descent classification performance. However, there is a large margin between both datasets showing the difficulty of YTOv2.2 dataset.

Ablation Studies. We performed an ablation study for key components of our loss function, using LayerCAM (Jiang et al., 2021) as baseline to generate CAMs for pseudo-labels (see Tab.3). We observe that using only pseudo-labels

²<https://www.youtube.com>

| Methods | YTOv1 | YTOv2.2 |
|---|-------------|-------------|
| CAM (Zhou et al., 2016) (<i>cvpr,2016</i>) | 85.3 | 73.9 |
| GradCAM (Selvaraju et al., 2017) (<i>iccv,2017</i>) | 85.3 | 71.3 |
| GradCAM++ (Chattopadhyay et al., 2018) (<i>wacv,2018</i>) | 84.4 | 72.4 |
| Smooth-GradCAM++ (Omeiza et al., 2019) (<i>corr,2019</i>) | 82.6 | 75.2 |
| XGradCAM (Fu et al., 2020) (<i>bmvc,2020</i>) | 87.3 | 71.6 |
| LayerCAM (Jiang et al., 2021) (<i>ieee,2021</i>) | 84.4 | 72.1 |
| TCAM (ours) | 84.4 | 72.1 |

Table 2: Classification accuracy (CL) on test set of YTOv1 (Prest et al., 2012) and YTOv2.2 (Kalogeiton et al., 2016) datasets.

improved the localization accuracy from 65.6% to 68.5%. Adding CRF helps localization, but using only size constraint did not provide much benefits compared to the baseline alone. Combining pseudo-labels, CRF, and size constraint yielded the best localization performance of 70.5% but without considering temporal dependency. Adding our temporal module, CAM-TMP, improves the localization accuracy up to 73%, indicating its benefit.

In addition, the impact of time range dependency is investigated (see Fig.3). As expected, considering previous frames ($n > 0$) helped in improving localization compared to looking only to instant frames ($n = 0$). However, long range dependency hampers the performance after $n = 1$. After $n = 4$, localization performance drops below the case of $n = 0$. This is thought to be caused by *object displacement*. Spatial locations in nearby frames cover typically the same objects. Therefore, ROI in CAMs are expected to land on same objects. Consequently, collecting ROI via Eq.1 is expected to be beneficial. However, moving to far away frames makes the same spatial location cover *different* objects, therefore collecting the wrong object. As a result, while our proposed module, *i.e.* CAM-TMP, can leverage temporal dependency in videos to improve localization, it is limited to short range frames. Nonetheless, using long range time dependency still yields better performance than the baseline method Layer-CAM (Jiang et al., 2021) (Fig.3). Based on our results, we recommend using short range dependency. We mention that such factor is strongly tied to the video frame rate. Using long range dependency in fast frame rate could be safe. However, slow frame rate should be considered with caution. We note that the information of video frame rate is not provided in the studied datasets.

Visual Results. Fig.4 illustrates prediction cases over labeled ground truth frames. Our method yields CAMs that tend to cover the entire object with a clear distinction between foreground and background. It deals well with multi-instances, and partially visible objects. The second row shows a concrete case where random sampling prevents overfitting over small and strong ROI (bottom-right), and allows other consistent and discriminative objects to emerge (boat at center) from

| Methods | CorLoc |
|---|-------------|
| Layer-CAM (Jiang et al., 2021) (<i>ieee,2021</i>) | 65.6 |
| Ours + $\mathbb{C}_t^+ + \mathbb{C}_t^-$ | 68.5 |
| $n = 0$ Ours + $\mathbb{C}_t^+ + \mathbb{C}_t^- + \text{CRF}$ | 69.6 |
| Ours + $\mathbb{C}_t^+ + \mathbb{C}_t^- + \text{ASC}$ | 66.2 |
| Ours + $\mathbb{C}_t^+ + \mathbb{C}_t^- + \text{CRF} + \text{ASC}$ | 70.5 |
| $n > 0$ Ours + $\mathbb{C}_t^+ + \mathbb{C}_t^- + \text{CRF} + \text{ASC} + \text{CAM-TMP}$ | 73.0 |
| Improvement | +7.4 |

Table 3: Localization accuracy (CorLoc) of TCAM with different losses on the YTOv1 test set.



Figure 3: Localization accuracy (CorLoc) of TCAM with different temporal dependencies n on the YTOv1 test set.

low activations. Fig.5 shows typical failure of our method. They manifest by over-activation over tiny objects, and spill to background. This is mainly caused by heavy presence of wrong ROI activations over the baseline CAM used to generate pseudo-labels. Unfortunately, dominant erroneous pseudo-labels in this case can lead to wrong localization in our method. Their early detection in the baseline CAM and dealing with them is of paramount importance for future extensions of this work. Such issues go under learning with noisy labels which is still an ongoing active domain (Song et al., 2022). This highlights the dependency of our method to the accuracy of the backbone CNN classifier, and baseline CAM. We provide in supplementary material demonstrative videos, in addition to our code.

Demonstrative Videos. For demonstration, we provide illustrative videos for localization using our method. Videos can be found on this Google drive link: <https://drive.google.com/drive/folders/1D8Dg0dJ35Vf5Tqej3K5ZWfQz3LhgeQt?usp=sharing>.

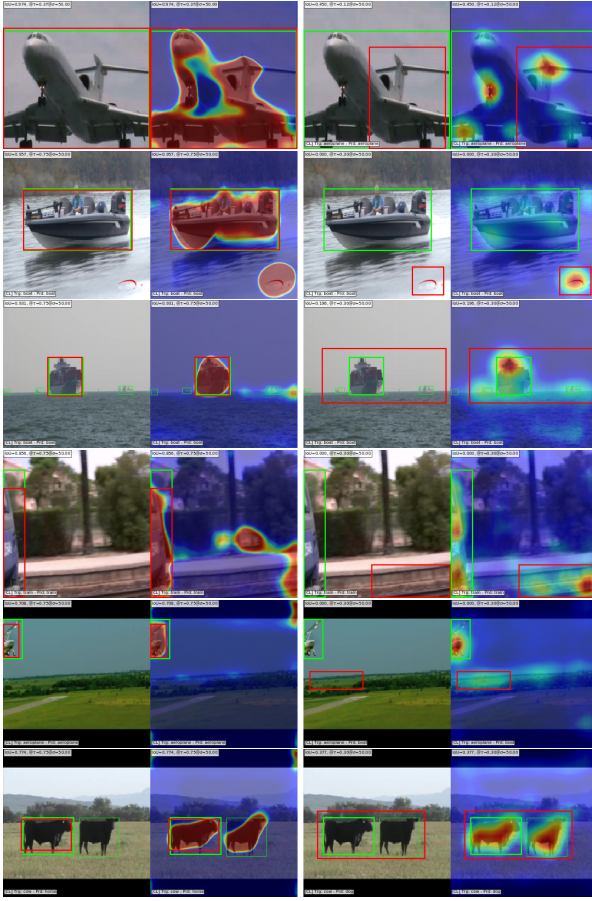


Figure 4: Prediction examples of test sets frames. *Left*: TCAM (ours). *Right*: baseline CAM method, LayerCAM (Jiang et al., 2021). *Bounding box*: ground truth (green), prediction (red). Second column is predicted CAM over image.

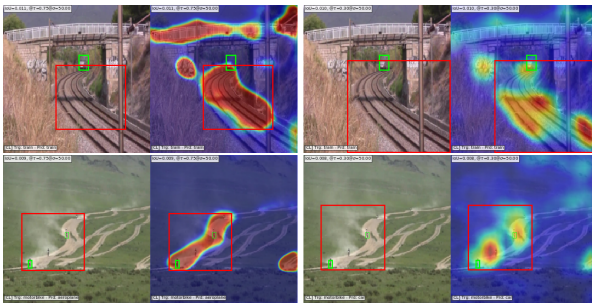


Figure 5: Typical failed cases of our method over test sets. *Left*: TCAM (ours). *Right*: baseline CAM method, LayerCAM (Jiang et al., 2021). *Bounding box*: ground truth (green), prediction (red). Second column is predicted CAM over image.

5 Conclusion

CAM-based methods have seen large success in still images for WSOL task. Due to several limitations in current work in WSVOL task, we propose to leverage CAMs for this task. However, since CAMs are not designed to benefit from temporal information in videos, we propose a new module, CAM-TMP, that allows CAMs to do so. It aims to collect available ROI from a sequence of CAMs, which are used to generate pseudo-labels for training. Combined with local and global constraints, we are able to train our model for WSVOL task. Evaluated on two public benchmarks for unconstrained videos, we demonstrated that simple CAM-methods can yield competitive results. Our method yielded new state-of-the-art localization performance. Our ablations show that localization improvement in our method can be done by leveraging short time dependency. Demonstrative videos suggest that our proposal can be easily adapted for subsequent tasks such as video object tracking and detection.

Acknowledgment

This research was supported in part by the Canadian Institutes of Health Research, the Natural Sciences and Engineering Research Council of Canada, and Compute Canada.

A Visual results

Fig.6, 7 present more prediction cases over labeled ground truth frames.

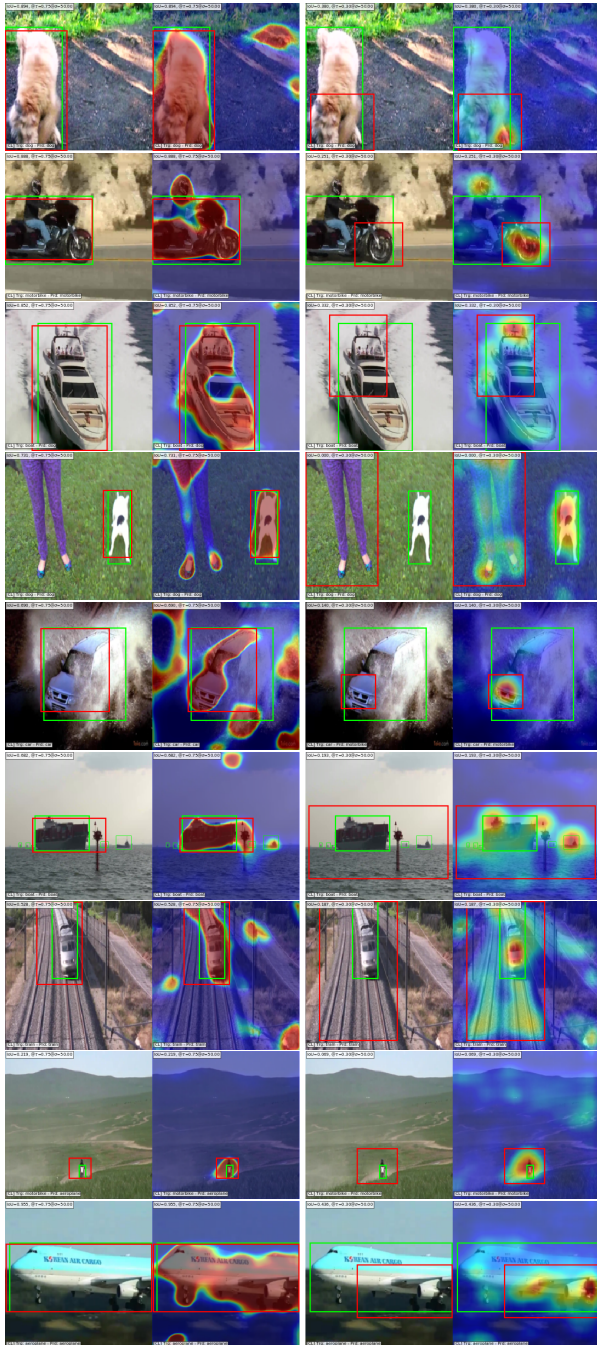


Figure 6: Prediction examples of test sets frames. *Left*: TCAM (ours). *Right*: baseline CAM method, LayerCAM (Jiang et al., 2021). *Bounding box*: ground truth (green), prediction (red). Second column is predicted CAM over image.

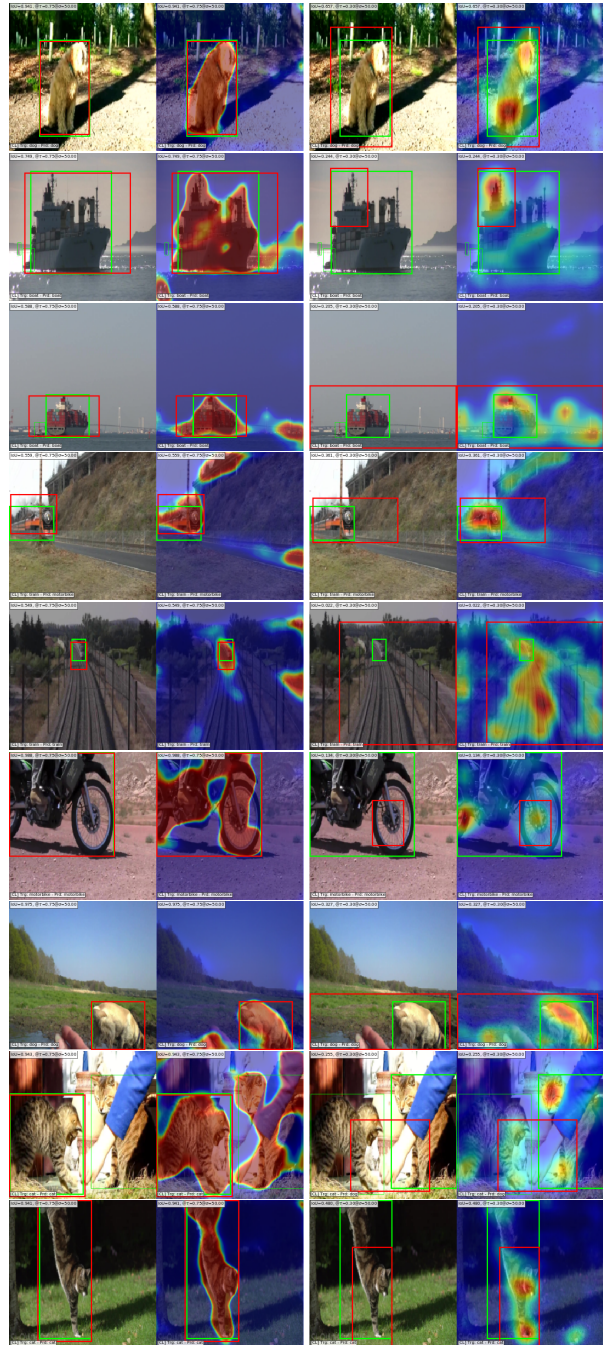


Figure 7: Prediction examples of test sets frames. *Left*: TCAM (ours). *Right*: baseline CAM method, LayerCAM (Jiang et al., 2021). *Bounding box*: ground truth (green), prediction (red). Second column is predicted CAM over image.

References

Adebayo, J., Gilmer, J., Muelly, M., Goodfellow, I., Hardt, M., and Kim, B. (2018). Sanity checks for saliency maps. In *NeurIPS*.

Alexe, B., Deselaers, T., and Ferrari, V. (2012). Measuring the objectness of image windows. *TPAMI*, 34(11):2189–2202.

Banica, D., Agape, A., Ion, A., and Sminchisescu, C. (2013). Video object segmentation by salient segment chain composition. In *ICCVW*.

Belharbi, S., Ben Ayed, I., McCaffrey, L., and Granger, E. (2019). Deep ordinal classification with inequality constraints. *CoRR*, abs/1911.10720.

Belharbi, S., Pedersoli, M., Ben Ayed, I., McCaffrey, L., and Granger, E. (2022a). Negative evidence matters in interpretable histology image classification. In *MIDL*.

Belharbi, S., Rony, J., Dolz, J., Ben Ayed, I., McCaffrey, L., and Granger, E. (2022b). Deep interpretable classification and weakly-supervised segmentation of histology images via max-min uncertainty. *IEEE Transactions on Medical Imaging*, 41:702–714.

Belharbi, S., Sarraf, A., Pedersoli, M., Ben Ayed, I., McCaffrey, L., and Granger, E. (2022c). F-cam: Full resolution class activation maps via guided parametric upscaling. In *WACV*.

Bergmann, P., Meinhardt, T., and Leal-Taixé, L. (2019). Tracking without bells and whistles. In *ICCV*.

Boyd, S. and Vandenberghe, L. (2004). *Convex optimization*. Cambridge university press.

Cao, C., Liu, X., Yang, Y., et al. (2015). Look and think twice: Capturing top-down visual attention with feedback convolutional neural networks. In *ICCV*.

Chang, X., Yang, Y., Long, G., Zhang, C., and Hauptmann, A. G. (2016). Dynamic concept composition for zero-example event detection. In *AAAI*.

Chattopadhyay, A., Sarkar, A., Howlader, P., and Balasubramanian, V. N. (2018). Grad-cam++: Generalized gradient-based visual explanations for deep convolutional networks. In *WACV*.

Chen, D., Chen, H., and Chang, L. (2012). Video object cosegmentation. In *Multimedia Conference*.

Chen, Y., Cao, Y., Hu, H., and Wang, L. (2020). Memory enhanced global-local aggregation for video object detection. In *CVPR*.

Choe, J., Oh, S. J., Lee, S., Chun, S., Akata, Z., and Shim, H. (2020). Evaluating weakly supervised object localization methods right. In *CVPR*.

Choe, J. and Shim, H. (2019). Attention-based dropout layer for weakly supervised object localization. In *CVPR*.

Croitoru, I., Bogolin, S.-V., and Leordeanu, M. (2019). Unsupervised learning of foreground object segmentation. *International Journal of Computer Vision*, 127(9):1279–1302.

Desai, S. and Ramaswamy, H. (2020). Ablation-cam: Visual explanations for deep convolutional network via gradient-free localization. In *WACV*.

Deselaers, T., Alexe, B., and Ferrari, V. (2012). Weakly supervised localization and learning with generic knowledge. *IJCV*, 100(3):275–293.

Durand, T., Mordan, T., Thome, N., and Cord, M. (2017). Wildcat: Weakly supervised learning of deep convnets for image classification, pointwise localization and segmentation. In *CVPR*.

Durand, T., Thome, N., and Cord, M. (2016). Weldon: Weakly supervised learning of deep convolutional neural networks. In *CVPR*.

Fu, H., Xu, D., Zhang, B., and Lin, S. (2014). Object-based multiple foreground video co-segmentation. In *CVPR*.

Fu, R., Hu, Q., Dong, X., Guo, Y., Gao, Y., and Li, B. (2020). Axiom-based grad-cam: Towards accurate visualization and explanation of cnns. In *BMVC*.

Gao, W., Wan, F., Pan, X., Peng, Z., Tian, Q., Han, Z., Zhou, B., and Ye, Q. (2021). TS-CAM: token semantic coupled attention map for weakly supervised object localization. In *ICCV*.

Haller, E. and Leordeanu, M. (2017). Unsupervised object segmentation in video by efficient selection of highly probable positive features. In *ICCV*.

Han, M., Wang, Y., Chang, X., and Qiao, Y. (2020). Mining inter-video proposal relations for video object detection. In *ECCV*.

Hartmann, G., Grundmann, M., Hoffman, J., Tsai, D., Kwatra, V., Madani, O., Vijayanarasimhan, S., Essa, I. A., Rehg, J. M., and Sukthankar, R. (2012). Weakly supervised learning of object segmentations from web-scale video. In *ECCV*.

He, K., Zhang, X., Ren, S., and Sun, J. (2016). Deep residual learning for image recognition. In *CVPR*.

Ilse, M., Tomczak, J., and Welling, M. (2018). Attention-based deep multiple instance learning. In *International conference on machine learning*, pages 2127–2136. PMLR.

Jerripothula, K. R., Cai, J., and Yuan, J. (2016). CATS: co-saliency activated tracklet selection for video co-localization. In *ECCV*.

Jiang, P., Zhang, C., Hou, Q., Cheng, M., and Wei, Y. (2021). Layer-cam: Exploring hierarchical class activation maps for localization. *IEEE Trans. Image Process.*, 30:5875–5888.

Joulin, A., Tang, K., and Fei-Fei, L. (2014). Efficient image and video co-localization with frank-wolfe algorithm. In *ECCV*.

Kalogeiton, V., Ferrari, V., and Schmid, C. (2016). Analysing domain shift factors between videos and images for object detection. *TPAMI*, 38(11):2327–2334.

Kervadec, H., Dolz, J., Yuan, J., Desrosiers, C., Granger, E., and Ben Ayed, I. (2019). Constrained deep networks: Lagrangian optimization via log-barrier extensions. *CoRR*, abs/1904.04205.

Ki, M., Uh, Y., Lee, W., and Byun, H. (2020). In-sample contrastive learning and consistent attention for weakly supervised object localization. In *ACCV*.

Kindermans, P.-J., Hooker, S., Adebayo, J., Alber, M., Schütt, K. T., Dähne, S., Erhan, D., and Kim, B. (2019). *The (Un)reliability of Saliency Methods*, pages 267–280.

Koh, Y. J., Jang, W., and Kim, C. (2016). POD: discovering primary objects in videos based on evolutionary refinement of object recurrence, background, and primary object models. In *CVPR*.

Kwak, S., Cho, M., Laptev, I., Ponce, J., and Schmid, C. (2015). Unsupervised object discovery and tracking in video collections. In *ICCV*.

Lee, J., Kim, E., Lee, S., Lee, J., and Yoon, S. (2019). Ficklenet: Weakly and semi-supervised semantic image segmentation using stochastic inference. In *CVPR*.

Lee, Y., Kim, J., and Grauman, K. (2011). Key-segments for video object segmentation. In *ICCV*.

Li, K., Wu, Z., Peng, K., et al. (2018). Tell me where to look: Guided attention inference network. In *CVPR*.

Lin, M., Chen, Q., and Yan, S. (2013). Network in network. *CoRR*, abs/1312.4400.

Liu, X., Tao, D., Song, M., Ruan, Y., Chen, C., and Bu, J. (2014). Weakly supervised multiclass video segmentation. In *CVPR*.

Luo, W., Xing, J., Milan, A., Zhang, X., Liu, W., and Kim, T. (2021). Multiple object tracking: A literature review. *Artificial Intelligence*, 293:103448.

Mai, J., Yang, M., and Luo, W. (2020). Erasing integrated learning: A simple yet effective approach for weakly supervised object localization. In *CVPR*.

Meethal, A., Pedersoli, M., Belharbi, S., and Granger, E. (2020). Convolutional stn for weakly supervised object localization and beyond. In *ICPR*.

Naidu, R., Ghosh, A., Maurya, Y., K, S. R. N., and Kundu, S. S. (2020). IS-CAM: integrated score-cam for axiomatic-based explanations. *CoRR*, abs/2010.03023.

Naidu, R. and Michael, J. (2020). SS-CAM: smoothed score-cam for sharper visual feature localization. *CoRR*, abs/2006.14255.

Omeiza, D., Speakman, S., Cintas, C., and Weldemariam, K. (2019). Smooth grad-cam++: An enhanced inference level visualization technique for deep convolutional neural network models. *CoRR*, abs/1908.01224.

Oquab, M., Bottou, L., Laptev, I., and Sivic, J. (2015). Is object localization for free?–weakly-supervised learning with convolutional neural networks. In *CVPR*.

Otsu, N. (1979). A threshold selection method from gray-level histograms. *IEEE Transactions on Systems, Man, and Cybernetics*, 9(1):62–66.

Papazoglou, A. and Ferrari, V. (2013). Fast object segmentation in unconstrained video. In *ICCV*.

Pathak, D., Krahenbuhl, P., and Darrell, T. (2015). Constrained convolutional neural networks for weakly supervised segmentation. In *ICCV*.

Pinheiro, P. and Collobert, R. (2015). From image-level to pixel-level labeling with convolutional networks. In *CVPR*.

Prest, A., Leistner, C., Civera, J., Schmid, C., and Ferrari, V. (2012). Learning object class detectors from weakly annotated video. In *CVPR*.

Rochan, M., Rahman, S., Bruce, N. D. B., and Wang, Y. (2016). Weakly supervised object localization and segmentation in videos. *Image and Vision Computing*, 56:1–12.

Ronneberger, O., Fischer, P., and Brox, T. (2015). U-net: Convolutional networks for biomedical image segmentation. In *MICCAI*.

Rony, J., Belharbi, S., Dolz, J., Ayed, I. B., McCaffrey, L., and Granger, E. (2022). Deep weakly-supervised learning methods for classification and localization in histology images: a survey. *CoRR*, abs/1909.03354.

Rother, C., Kolmogorov, V., and Blake, A. (2004). "grabcut": interactive foreground extraction using iterated graph cuts. *ACM Transactions on Graphics*, 23(3):309–314.

Selvaraju, R. R., Cogswell, M., Das, A., Vedantam, R., Parikh, D., and Batra, D. (2017). Grad-cam: Visual explanations from deep networks via gradient-based localization. In *ICCV*.

Shao, F., Chen, L., Shao, J., Ji, W., Xiao, S., Ye, L., Zhuang, Y., and Xiao, J. (2022). Deep learning for weakly-supervised object detection and localization: A survey. *Neurocomputing*, 496:192–207.

Singh, K. and Lee, Y. (2017). Hide-and-seek: Forcing a network to be meticulous for weakly-supervised object and action localization. In *ICCV*.

Song, H., Kim, M., Park, D., Shin, Y., and Lee, J.-G. (2022). Learning from noisy labels with deep neural networks: A survey. *IEEE Transactions on Neural Networks and Learning Systems*.

Stretcu, O. and Leordeanu, M. (2015). Multiple frames matching for object discovery in video. In *BMVC*.

Sun, C., Paluri, M., Collobert, R., Nevatia, R., and Bourdev, L. (2016). Pronet: Learning to propose object-specific boxes for cascaded neural networks. In *CVPR*.

Sundaram, N., Brox, T., and Keutzer, K. (2010). Dense point trajectories by gpu-accelerated large displacement optical flow. In *ECCV*.

Tang, K., Sukthankar, R., Yagnik, J., and Fei-Fei, L. (2013). Discriminative segment annotation in weakly labeled video. In *CVPR*.

Tang, M., Perazzi, F., Djelouah, A., Ben Ayed, I., Schroers, C., and Boykov, Y. (2018). On regularized losses for weakly-supervised cnn segmentation. In *ECCV*.

Tokmakov, P., Alahari, K., and Schmid, C. (2016). Weakly-supervised semantic segmentation using motion cues. In *ECCV*.

Tsai, Y.-H., Zhong, G., and Yang, M.-H. (2016). Semantic co-segmentation in videos. In *ECCV*.

Umer, S., Dawood, H., Yousaf, M. H., Dawood, H., and Ahmad, H. (2021). Efficient foreground object segmentation from video by probability weighted moments. *Optik*, 229:166251.

Wang, H., Wang, Z., Du, M., Yang, F., Zhang, Z., Ding, S., Mardziel, P., and Hu, X. (2020). Score-cam: Score-weighted visual explanations for convolutional neural networks. In *CVPR workshop*.

Wei, J., Wang, Q., Li, Z., Wang, S., Zhou, S. K., and Cui, S. (2021). Shallow feature matters for weakly supervised object localization. In *CVPR*.

Wei, Y., Feng, J., Liang, X., Cheng, M.-M., Zhao, Y., and Yan, S. (2017). Object region mining with adversarial erasing: A simple classification to semantic segmentation approach. In *CVPR*.

Xu, C., Xiong, C., and Corso, J. J. (2012). Streaming hierarchical video segmentation. In *ECCV*.

Xue, H., Liu, C., Wan, F., Jiao, J., Ji, X., and Ye, Q. (2019). Danet: Divergent activation for weakly supervised object localization. In *ICCV*.

Yan, Y., Xu, C., Cai, D., and Corso, J. J. (2017). Weakly supervised actor-action segmentation via robust multi-task ranking. In *CVPR*.

Yang, S., Kim, Y., Kim, Y., and Kim, C. (2020). Combinational class activation maps for weakly supervised object localization. In *WACV*.

Yun, S., Han, D., Chun, S., Oh, S., Yoo, Y., and Choe, J. (2019). Cutmix: Regularization strategy to train strong classifiers with localizable features. In *ICCV*.

Zhang, C., Cao, Y., and Wu, J. (2020a). Rethinking the route towards weakly supervised object localization. In *CVPR*.

Zhang, D., Han, J., Jiang, L., Ye, S., and Chang, X. (2017). Revealing event saliency in unconstrained video collection. *IEEE Trans. Image Process.*, 26(4):1746–1758.

Zhang, D., Han, J., Yang, L., and Xu, D. (2020b). Spftn: A joint learning framework for localizing and segmenting objects in weakly labeled videos. *TPAMI*, 42(2):475–489.

Zhang, D., Javed, O., and Shah, M. (2014). Video object co-segmentation by regulated maximum weight cliques. In *ECCV*.

Zhang, J., Bargal, S. A., Lin, Z., et al. (2018a). Top-down neural attention by excitation backprop. *International Journal of Computer Vision*, 126(10):1084–1102.

Zhang, X., Wei, Y., Feng, J., Yang, Y., and Huang, T. (2018b). Adversarial complementary learning for weakly supervised object localization. In *CVPR*.

Zhang, X., Wei, Y., Kang, G., Yang, Y., and Huang, T. (2018c). Self-produced guidance for weakly-supervised object localization. In *ECCV*.

Zhang, X., Wei, Y., and Yang, Y. (2020c). Inter-image communication for weakly supervised localization. In Vedaldi, A., Bischof, H., Brox, T., and Frahm, J., editors, *ECCV*, Lecture Notes in Computer Science.

Zhang, Y., Chen, X., Li, J., Wang, C., and Xia, C. (2015). Semantic object segmentation via detection in weakly labeled video. In *CVPR*.

Zhou, B., Khosla, A., Lapedriza, A., Oliva, A., and Torralba, A. (2016). Learning deep features for discriminative localization. In *CVPR*.

Zhou, Y., Zhu, Y., Ye, Q., Qiu, Q., and Jiao, J. (2018). Weakly supervised instance segmentation using class peak response. In *CVPR*.

Zhu, Y., Zhou, Y., Ye, Q., et al. (2017). Soft proposal networks for weakly supervised object localization. In *ICCV*.